Discrete non–local boundary conditions for Split–Step Padé Approximations of the One–Way Helmholtz Equation

Matthias Ehrhardt [*,1] and Andrea Zisowsky [1]

Institut für Mathematik, Technische Universität Berlin, Strasse des 17. Juni 136, D–10623 Berlin, Germany

Abstract

This paper deals with the efficient numerical solution of the two–dimensional one–way Helmholtz equation posed on an unbounded domain. In this case one has to introduce artificial boundary conditions to confine the computational domain. The main topic of this work is the construction of so–called discrete transparent boundary conditions for state-of-the-art parabolic equations methods, namely a split–step discretization of the high–order parabolic approximation and the split–step Padé algorithm of Collins. Finally, several numerical examples arising in optics and underwater acoustics illustrate the efficiency and accuracy of our approach.

Key words: split–step method, Padé approximation, finite difference method, one–way Helmholtz equation, discrete transparent boundary conditions
PACS: 02.70.Bf, 31.15.Fx, 42.82.-m, 43.30.+m, 92.10.Vz

1 Introduction

In this work we study two numerical methods for two–dimensional scalar wave propagation problems. These problems are usually modeled by the Helmholtz equation posed on an unbounded domain in $\mathbb{R}^2$ and typical applications are

* Corresponding author.
Email addresses: ehrhardt@math.tu-berlin.de (Matthias Ehrhardt), zisowsky@math.tu-berlin.de (Andrea Zisowsky).
URLs: http://www.math.tu-berlin.de/~ehrhardt/ (Matthias Ehrhardt), http://www.math.tu-berlin.de/~zisowsky/ (Andrea Zisowsky).
[1] Supported by the DFG Research Center MATHEON "Mathematics for key technologies" in Berlin.

integrated optics [46], seismic migration [9] and underwater acoustics [28]. E.g. in seismology images of geological formations are constructed by the downward computation of sound wave reflection data measured at the surface. Generally the full Helmholtz equation in $\mathbb{R}^2$ is solved as a boundary value problem with radiation boundary conditions [30]. Alternative strategies are boundary integral methods (BIM) [1], infinite elements (IFE) [21] and perfectly matched layer (PML) [6] approaches. We note that the same strategies are used if the governing equation has an extended length scale in one spatial direction. This is the case e.g. in integrated optics [46] where the numerical solution is seeked for photonic devices with a propagation distance of some millimeters whereas the transverse length scale is typically only a few micrometers.

However, in many situations one can distinguish a main propagation direction and factorize the Helmholtz equation if the wavenumber is assumed to be constant. This procedure leads to the *one–way Helmholtz equation*. Different one–way approximations yield various so–called *Beam Propagation Methods (BPM)* in optics [18] or *Parabolic Equation (PE)* methods in (underwater and aero) acoustics [44]. In the sequel we will use a notation common to the application in underwater acoustics. Nevertheless our approach is generally applicable to all one–way wave propagation problems in 2D and we will discuss a numerical example from optics in §7.

In *underwater acoustics* one wants to calculate the underwater acoustic pressure $p(z,r)$ emerging from a time–harmonic point source of time dependence $\exp(-i2\pi ft)$ located in the water at $(z_s,0)$. Here, $r>0$ denotes the radial range variable, $0<z<z_b$ the depth variable and f denotes the (usually low) frequency of the emitted sound. The water surface is at $z=0$, and the (horizontal) sea bottom at $z=z_b$. We denote the local sound speed by $c(z,r)$, the density by $\rho(z,r)$, and the attenuation by $\alpha(z,r)\geq 0$. $n(z,r)=c_0/c(z,r)$ is the refractive index, with a reference sound speed c_0 (usually the smallest sound speed in the model). The environmental layout of the problem is illustrated in Figure 1.

The starting point of our consideration is the *Helmholtz equation* ('far–field equation') for a variable–density medium and a time–harmonic point source

$$\frac{1}{r}\frac{\partial}{\partial r}\left(r\,\frac{\partial p}{\partial r}\right)+\rho\,\frac{\partial}{\partial z}\left(\rho^{-1}\,\frac{\partial p}{\partial z}\right)+k_0^2N^2p=0,\qquad r>0, \tag{1}$$

with the *complex refractive index*

$$N(z,r)=n(z,r)+i\alpha(z,r)/k_0,$$

and the reference wave number $k_0=2\pi f/c_0$. In the *far–field approximation*

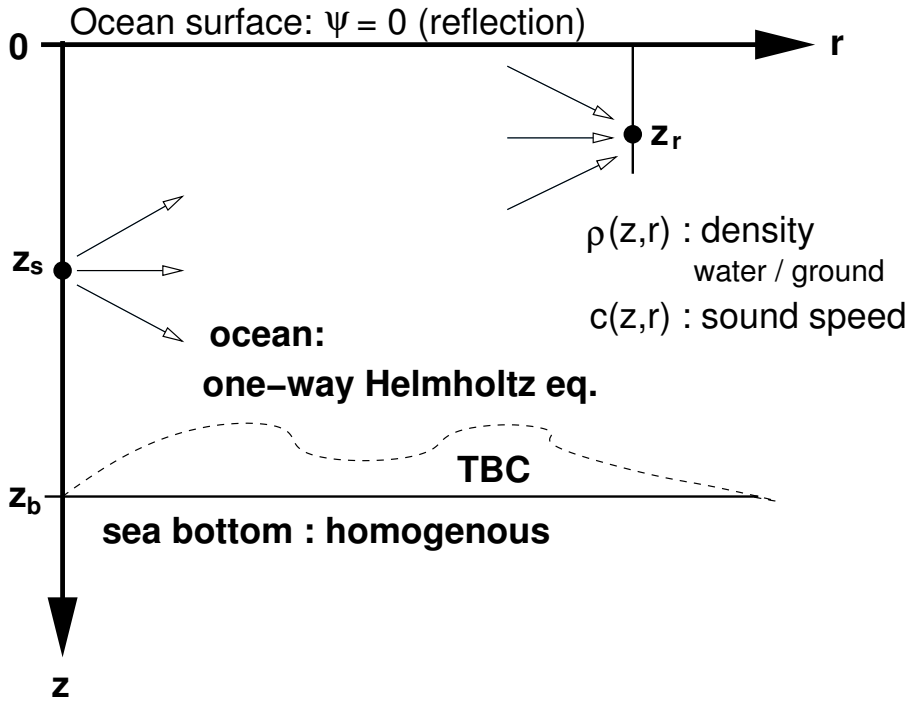

Fig. 1. Time–harmonic acoustic waves are emitted from the source at depth z_s and measured/numerically simulated at a receiver at depth z_r.

($k_0 r \gg 1$) the (complex valued) *outgoing acoustic field*

$$\psi(z,r) = \sqrt{k_0 r}\, p(z,r)\, e^{-ik_0 r} \tag{2}$$

satisfies the *one–way Helmholtz equation*:

$$\psi_r = ik_0\Big(-1 + \sqrt{1-L}\Big)\psi, \qquad r > 0. \tag{3}$$

Here, $\sqrt{1-L}$ is a pseudo–differential operator, and L the *Schrödinger operator* ('depth operator')

$$L = -k_0^{-2}\rho\,\partial_z(\rho^{-1}\partial_z) + V(z,r) \tag{4}$$

with the *complex valued "potential"* $V(z,r) = 1 - N^2(z,r)$.

The evolution equation (3) is much easier to solve numerically and requires far less memory than the elliptic Helmholtz equation (1). Hence, (3) forms the basis for all standard linear models in underwater acoustics (normal mode, ray representation, parabolic equation). Strictly speaking, (3) is only valid for horizontally stratified oceans, i.e. for range–independent parameters c, ρ, and α. In practice, however, it is still used in situations with weak range dependence, and backscatter is neglected.

An efficient solution method for (3) is the *split–step Fourier method* [26], [19] which computes the square root operator directly in the transformed Fourier space and allows large range and depth steps. However, *Higher–order PEs* han-

dle wide propagation angles and variations of the refractive index (especially at the water–bottom interface) more accurately than the split–step Fourier solution. These *Padé "Parabolic" approximations* of the one–way Helmholtz equation (3) consist in formally approximating the pseudo–differential square root operator $\sqrt{1-L}$ by a (ℓ, m)–Padé approximant:

$$\psi_r = ik_0\Big(\frac{P_\ell(L)}{Q_m(L)} - 1\Big)\psi, \qquad r > 0. \tag{5}$$

Here P_ℓ, Q_m denote polynomials of degree ℓ, m, respectively. While the Padé approximation is the most usual method, it is inaccurate near the singularity of the square root operator. Other reasonable candidates for the approximation are the Chebyshev (L^∞) approximation, the least squares (L^2) approximation and the Chebyshev–Padé approximation [22]. Standard numerical solution methods for (5) uses finite differences or finite elements and are relatively inefficient since they tend to require a rather small grid spacing (compared to the split–step Fourier method). The *split–step Padé method* combines both benefits: the efficiency of the split–step Fourier method and the accuracy of the higher–order PEs. This algorithm is orders of magnitudes faster than standard finite difference methods and includes higher–order asymptotics. Furthermore, it allows for a powerful parallel implementation.

In this article we shall focus on adequate boundary conditions (BCs) at the sea–bottom for finite difference discretizations of equations of the form (5) and for the split–step Padé method to solve (3). The presented approach generalizes our previously obtained results for the special case of a (1,1)–Padé approximant [3]. At the free water surface one usually employs a Dirichlet ("pressure release") BC: $\psi(z = 0, r) = 0$. At the sea bottom the wave propagation in water has to be coupled to the wave propagation in the sediments of the bottom. The bottom will be modeled as the homogeneous half–space region $z > z_b$ with constant parameters c_b, ρ_b, and α_b.

In practical simulations one is only interested in the acoustic field $\psi(z, r)$ in the water, i.e. for $0 < z < z_b$. While the physical problem is posed on the unbounded z–interval $(0, \infty)$, one wishes to restrict the computational domain in the z–direction by introducing an artificial boundary at or shortly below the sea bottom. This artificial BC should of course change the model as little as possible. Hitherto, the standard strategy was to introduce rather thick *absorbing layers* below the sea bottom and then to limit the z–range by again imposing a Dirichlet BC [28]. With a carefully designed absorption profile and layer thickness [7] this technique produces accurate results at the expense of an increased computational domain. Absorbing layer strategies increase the computational costs, for PE simulations typically by a factor around 2 [32]. However, in simulations without attenuation ("false absorbing layer method") [32] much thicker absorbing layers have been used to ensure accuracy and, respectively, numerical stability.

Papadakis derived in [39], [40] *impedance BCs* or *transparent boundary conditions* (TBCs) for the (1,0) and (1,1)–Padé approximant which completely solves the problem of restricting the z–domain without changing the physical model: complementing the PE with a TBC at z_b allows to recover — on the finite computational domain $(0, z_b)$ — the exact half–space solution on $0 < z < \infty$. As the (1,0)–Padé approximant is a *Schrödinger equation*, similar strategies have been developed independently for various application fields [2], [5], [27], [35], [43]. While these early TBCs assumed a homogeneous region behind the artificial boundary, recently TBCs for a media with linear depth dependence of the refraction index [16], [29], [34], [12] were obtained.

Towards the end of this introduction we shall now turn to the main motivation of this paper. While TBCs fully solve the problem of cutting off the z–domain for the analytical equation, their numerical discretization is far from trivial. Indeed, all available discretizations are less accurate than the discretized half–space problem and they render the overall numerical scheme only conditionally stable [36]. Additionally, all available TBCs are derived for low–order PEs which have very limited wide–angle capabilities and are insufficient for many shallow–water problems. In [41] a TBC was derived for the one–way Helmholtz equation (3) which has (formally) unlimited wide–angle capability. This TBC (in a similar formulation) was implemented by Brooke and Thomson [8] and exposed computational instabilities.

The object of this paper is to construct exact *discrete transparent boundary conditions* (DTBCs) for state-of-the-art PE models, namely a split–step discretization of the high–order parabolic equations (5) and the split–step Padé solution method of Collins [10]. With these DTBCs the overall scheme is as accurate as the discretized half–space problem (up to some very small round–off errors and evanescent errors in the numerical inverse $\mathcal{Z}$–transformation). We remark that a similar approach for the OWWE (*one–way wave equation*) of Godin [24] was done by Mikhin [38] and also refer the reader to a *semi–discrete TBC* by Schmidt et al. [42] based on a Laplace–transformation in the depth variable.

The paper is organized as follows: we will review in §2 the high–order PEs and propose in §3 a semi–discrete evolution equation. Alternatively, we present in §4 the well–known *split–step Padé algorithm* of Collins [10]. To solve the resulting schemes numerically it remains to discretize adequately the Schrödinger operator L in depth (transverse) direction in §5. In §6 the DTBCs are derived directly for the proposed numerical methods of §3, §4. Finally, we conclude in §7 with several numerical examples from optics and underwater acoustics showing the effectiveness and accuracy of our DTBCs. In our numerical tests of DTBCs (in §7) we will only deal with horizontal bottoms. However, irregular bottom surfaces and sub–bottom layers can be included by simply extending the range of z.

2 The Higher–Order Parabolic Equations

Padé "Parabolic" approximations of (3) consist in formally approximating the pseudo–differential square root operator $\sqrt{1-L}$ by rational functions of L:

$$\sqrt{1-\lambda} \approx \frac{p_0 - p_1\lambda + p_2\lambda^2 - ... + p_l\lambda^l}{1 - q_1\lambda + q_2\lambda^2 - ... + q_m\lambda^m} =: \frac{P_\ell(\lambda)}{Q_m(\lambda)}. \tag{6}$$

This approach yields a PDE that is easier to discretize than the pseudo–differential equation (3). The coefficients above can be easily determined using a symbolic mathematical software, e.g. in the MAPLE package the function call

```
l:=2; m:=2;
with(numapprox):pade(sqrt(1-lambda), lambda, [l,m]);
```

yields the desired values for the (l, m)–Padé approximant (6). We remark that the most accurate of these approximations are obtained from $l = m$ or $l = m + 1$, cf. [45].

Let us briefly review the well–known low–order PEs. The linear approximation of $\sqrt{1-\lambda}$ by $1 - \lambda/2$ gives the *narrow angle* or *standard "parabolic" equation* of Tappert [44]

$$\psi_r = -\frac{ik_0}{2} L\psi, \qquad r > 0.$$

This *Schrödinger equation* is a reasonable description of waves with a propagation direction within about 10–15° off the horizontal. We note that this PE was introduced by Leontovich and Fock [33] in 1946 to the problem of radio wave propagation in the atmosphere. Rational approximations of the form

$$\sqrt{1-\lambda} \approx \frac{p_0 - p_1\lambda}{1 - q_1\lambda},$$

with real p_0, p_1, q_1 yield the *wide angle "parabolic" equations* (WAPE)

$$\psi_r = ik_0 \left(\frac{p_0 - p_1 L}{1 - q_1 L} - 1 \right) \psi, \qquad r > 0. \tag{7}$$

With the special choice $p_0 = 1$, $p_1 = \frac{3}{4}$, $q_1 = \frac{1}{4}$ ((1,1)–Padé approximant of $\sqrt{1-\lambda}$) one obtains the *WAPE of Claerbout* ("standard 40° equation") [9]. In [23] Greene determines these coefficients by minimizing the approximation error of $\sqrt{1-\lambda}$ over suitable λ–intervals

$$\sqrt{1-\lambda} \approx \frac{0.99987 - 0.79624\lambda}{1 - 0.30102\lambda}.$$

These WAPE models furnish a much better description of the wave propagation up to angles of about 40°. Applying a (2,2)–Padé approximant

$$\sqrt{1-\lambda} \approx \frac{1-\frac{5}{4}\lambda+\frac{5}{16}\lambda^2}{1-\frac{3}{4}\lambda+\frac{1}{16}\lambda^2}$$

yields a *wider–angle PE* valid to nearly 55° from the main propagation direction. An overview of several approximations is given in [25]. For a concise discussion of possible numerical instabilities associated with evanescent modes that are exited when approximating a range–dependent medium by a piecewise uniform waveguide structures ('staircase approximation') we refer to [47] and the references therein.

3 The semi–discrete evolution equation

First we discretize in range (which is the principal propagation direction) using a *Crank–Nicolson type* (i.e. implicit midpoint) second–order discretization:

$$D_k^+\psi^n(z) = ik_0\Big(-1+\sqrt{1-L}\Big)\psi^{n+1/2}(z), \qquad n \geq 0, \tag{8}$$

with the usual forward difference operator $D_k^+\psi^n(z) = (\psi^{n+1}(z)-\psi^n(z))/k$ and the average $\psi^{n+1/2}(z) := (\psi^{n+1}(z)+\psi^n(z))/2$. Here, $\psi^n(z) \sim \psi(z, r_n)$, with the uniform range grid $r_n = nk$, $(k = \Delta r)$. This discretization results in

$$\Big(1+\frac{ik_0}{2}k\Big(1-\sqrt{1-L}\Big)\Big)\psi^{n+1}(z) = \Big(1-\frac{ik_0}{2}k\Big(1-\sqrt{1-L}\Big)\Big)\psi^n(z), \quad n \geq 0.$$

Now using the Padé approximant (6) of the square root operator yields

$$\begin{aligned}\Big(\Big(1+\frac{ik_0}{2}k\Big)Q_m(L) - \frac{ik_0}{2}kP_\ell(L)\Big)\psi^{n+1}(z) \\ = \Big(\Big(1-\frac{ik_0}{2}k\Big)Q_m(L) + \frac{ik_0}{2}kP_\ell(L)\Big)\psi^n(z), \quad n \geq 0,\end{aligned}$$

which can be written as the *semi–discrete evolution equation*

$$\psi^{n+1}(z) = \frac{U(L)}{W(L)}\,\psi^n(z), \quad n \geq 0, \tag{9}$$

with the polynomials $U(L)$, $W(L)$ of degree $p = \max(\ell, m)$:

$$\begin{aligned}U(L) &= \Big(1-\frac{ik_0}{2}k\Big)Q_m(L) + \frac{ik_0}{2}kP_\ell(L), \\ W(L) &= \Big(1+\frac{ik_0}{2}k\Big)Q_m(L) - \frac{ik_0}{2}kP_\ell(L).\end{aligned}$$

Using this ratio of polynomials as a higher–order parabolic equation (as it was done in [31]) is difficult to implement because powers of L are involved. Thus we introduce a *multiplicative splitting* (like in [42]) and write the evolution equation (9) in the following form (involving only first powers of L):

$$\psi^{n+1}(z) = \frac{c_U}{c_W} \prod_{l=1}^{p} \frac{1 - a_{l,p}L}{1 - b_{l,p}L} \, \psi^n(z), \quad n \geq 0, \tag{10}$$

once the polynomials U, W are factorized as

$$U(L) = c_U \prod_{l=1}^{p} (1 - a_{l,p}L), \quad W(L) = c_W \prod_{l=1}^{p} (1 - b_{l,p}L),$$

with some constants c_U, c_W.

The next step is to rewrite equation (10) of order $2p$ as a system of p second order differential equations. To do so, we introduce the *intermediate functions* $\varphi_1^{n+1}(z), \ldots, \varphi_{p-1}^{n+1}(z)$ that fulfill

$$\begin{aligned}
\varphi_1^{n+1}(z) &= \frac{1 - a_{1,p}L}{1 - b_{1,p}L} \, \psi^n(z), \\
\varphi_l^{n+1}(z) &= \frac{1 - a_{l,p}L}{1 - b_{l,p}L} \, \varphi_{l-1}^{n+1}(z), \quad l = 2, \ldots, p-1, \\
\psi^{n+1}(z) &= \frac{c_U}{c_W} \frac{1 - a_{p,p}L}{1 - b_{p,p}L} \, \varphi_{p-1}^{n+1}(z).
\end{aligned}$$

Thus, the system of p second order differential equations reads

$$\begin{aligned}
a_{1,p}L\psi^n(z) - b_{1,p}L\varphi_1^{n+1}(z) &= \psi^n(z) - \varphi_1^{n+1}(z), \\
a_{l,p}L\varphi_{l-1}^{n+1}(z) - b_{l,p}L\varphi_l^{n+1}(z) &= \varphi_{l-1}^{n+1}(z) - \varphi_l^{n+1}(z), \quad l = 2, \ldots, p-1, \\
\frac{c_U}{c_W} a_{p,p}L\varphi_{p-1}^{n+1}(z) - b_{p,p}L\psi^{n+1}(z) &= \frac{c_U}{c_W}\varphi_{p-1}^{n+1}(z) - \psi^{n+1}(z).
\end{aligned} \tag{11}$$

4 The Split–Step Padé solution method

In [10] Collins proposed the *split–step Padé algorithm*. The idea is to interchange the two steps of using the Padé approximation and solving the one–way Helmholtz equation (3). Thus, we first solve formally the one–way Helmholtz equation (3): if the field is known at the range $r_n = nk$ then the solution of (3) at range r_{n+1} is given by

$$\psi^{n+1} = \exp\left\{ik_0\Delta r\left(-1 + \sqrt{1 - L}\right)\right\} \psi^n, \qquad n \geq 0. \tag{12}$$

Afterwards we apply the Padé approximation to the operator that propagates the solution in range ('propagator'):

$$\exp\left\{ik_0\Delta r\left(-1+\sqrt{1-L}\right)\right\} \approx 1+\sum_{l=1}^{p}\frac{a_{l,p}L}{1+b_{l,p}L} = \prod_{l=1}^{n}\frac{1+\lambda_{l,p}L}{1+\mu_{l,p}L}. \tag{13}$$

Inserting (13) into (12) we get the *split–step Padé solution*

$$\psi^{n+1} = \psi^n + \sum_{l=1}^{p}\frac{a_{l,p}L}{1+b_{l,p}L}\,\psi^n, \qquad n \geq 0. \tag{14}$$

Remark 1 *The product formulation in* (13)*:*

$$\psi^{n+1} = \prod_{l=1}^{p}\frac{1+\lambda_{l,p}L}{1+\mu_{l,p}L}\,\psi^n, \qquad n \geq 0. \tag{15}$$

does not allow for parallel computations and hence we will focus in the sequel on the common additive formulation (14)*. The coefficients $\lambda_{l,p}$ and $\mu_{l,p}$ are complex conjugate (see [4]).*

5 The depth discretization

To solve (14) numerically it remains to discretize the depth operator L (4) w.r.t. the depth variable z (denoted by L_h). This is done using the approach of [3]:

$$L_h\psi_j^n = -k_0^{-2}\rho_j D^0_{\frac{h}{2}}(\rho_j^{-1}D^0_{\frac{h}{2}})\psi_j^n + V_j^n\psi_j^n. \tag{16}$$

Here, we used the notation $\psi_j^n \sim \psi^n(z_j)$, $z_j = jh$, $(h = \Delta z)$ and the centered difference quotient

$$D^0_{\frac{h}{2}}\psi_j^n = \frac{\psi^n_{j+\frac{1}{2}} - \psi^n_{j-\frac{1}{2}}}{h}.$$

In a *homogeneous waveguide* (i.e. $\rho = \text{const.}$, $c \equiv c_0$) without attenuation the discrete depth operator reduces to $L_h = -k_0^{-2}D_h^2$, with the standard second order difference quotient

$$D_h^2\psi_j^n = \frac{\psi^n_{j+1} - 2\psi_j^n + \psi^n_{j-1}}{h^2} = \partial_z^2\psi^n(z_j) + \mathrm{O}(h^2).$$

Collins showed in [10] how to adapt the split–step Padé technique for the discretized depth operator L_h. In the sequel we briefly review this idea.

We obtain formally from the taylor series

$$\psi^n(z_{j\pm1}) = \exp(\pm h\partial_z)\psi^n(z_j) = \exp\left(\mp hk_0L^{1/2}\right)\psi^n(z_j)$$

the expression

$$L_h = 2\frac{\cosh\left(\tau L^{1/2}\right) - 1}{\tau^2}, \quad \tau = hk_0. \tag{17}$$

Using the inverse function of cosh we obtain L as a function of L_h:

$$L = \Gamma(L_h) = \tau^{-2}\log^2\left[1 + \frac{\tau^2}{2}L_h + \sqrt{\left(1 + \frac{\tau^2}{2}L_h\right)^2 - 1}\right], \tag{18}$$

and inserting (18) into (12) gives

$$\psi_j^{n+1} = \exp\left\{ik_0\Delta r\left(-1 + \sqrt{1 - \Gamma(L_h)}\right)\right\}\psi_j^n, \qquad n > 0. \tag{19}$$

We proceed analogously to (13) and apply the Padé approximation

$$\exp\left\{ik_0\Delta r\left(-1 + \sqrt{1 - \Gamma(L_h)}\right)\right\} \approx 1 + \sum_{l=1}^{p}\frac{\tilde{a}_{l,p}L_h}{1 + \tilde{b}_{l,p}L_h}. \tag{20}$$

Finally, inserting (20) into (19) we get

$$\psi_j^{n+1} = \psi_j^n + \sum_{l=1}^{p}\frac{\tilde{a}_{l,p}L_h}{1 + \tilde{b}_{l,p}L_h}\,\psi_j^n, \qquad n > 0. \tag{21}$$

In order to compute the coefficients $\tilde{a}_{l,p}$, $\tilde{b}_{l,p}$, $l = 1, \ldots, p$ we compare the of both sides of (20). Therefore, we use the the taylor series

$$\Gamma(L_h) = \sum_{l=1}^{\infty}\gamma_l^{-1}\tau^{2l-2}L_h^l, \tag{22}$$

and obtain a system of nonlinear equations, that we solve by the MATLAB routine `fsolve`. In preparation therefore the coefficients γ_l and the taylor expansion of the l.h.s. in (20) were calculated using the symbolic package MAPLE.

6 The Discrete Transparent Boundary Conditions

In this section we will construct the discrete transparent boundary conditions (DTBCs) for the high–order PE and for the split-step Padé algorithm. The DTBCs are obtained by $\mathcal{Z}$–transformation of the fully discrete numerical schemes in the (homogeneous) fluid bottom region $j \geq J$. For the following derivations we make the basic assumption that the initial data $\psi^I = \psi(z, 0)$, which models a point source located at $(z_s, 0)$, is supported in the *interior domain* $0 < z < z_b$, i.e. $\operatorname{supp}\psi^I \subset (0, z_b)$. Approaches to overcome this restriction can be found in [17], [38].

We consider the system (11) with L replaced by L_h from (16) and drop for simplicity the second index p. In the exterior domain ($j \geq J$) the density is constant and we denote the constant potential in the bottom region with V_b. Thus the discrete depth operator L_h simplifies to $L_h\psi_j^n = -k_0^{-2}D_h^2\psi_j^n + V_b\psi_j^n$, $j \geq J$. Hence, the discrete system of p second order difference equations reads for $j \geq J$:

$$\begin{aligned}
-a_1 D_h^2\psi_j^n + b_1 D_h^2\varphi_{1,j}^{n+1} &= k_0^2(1-a_1V_b)\psi_j^n - k_0^2(1-b_1V_b)\varphi_{1,j}^{n+1},\\
-a_l D_h^2\varphi_{l-1,j}^{n+1} + b_l D_h^2\varphi_{l,j}^{n+1} &= k_0^2(1-a_lV_b)\varphi_{l-1,j}^{n+1} - k_0^2(1-b_1V_b)\varphi_{l,j}^{n+1},\\
&\qquad l = 2,\ldots,p-1,\\
-\frac{c_U}{c_W}a_p D_h^2\varphi_{p-1,j}^{n+1} + b_p D_h^2\psi_j^{n+1} &= \frac{c_U}{c_W}k_0^2(1-a_pV_b)\varphi_{p-1,j}^{n+1} - k_0^2(1-b_pV_b)\psi_j^{n+1}.
\end{aligned}$$

To solve this system we use the *$\mathcal{Z}$–transformation* [13]

$$\mathcal{Z}\{\varphi_j^n\} = \hat{\varphi}_j(z) := \sum_{n=0}^{\infty}\zeta^{-n}\varphi_j^n, \quad \zeta \in \mathbb{C}, \quad |\zeta| > R_{\varphi_j}, \tag{23}$$

where R_{φ_j} denotes the convergence radius of this Laurent series. Note that we denoted in (23) the transformation variable with ζ in order to assign z for the depth variable. This yields the following $\mathcal{Z}$–transformed system

$$\begin{aligned}
-a_1 D_h^2\hat{\psi}_j + \zeta b_1 D_h^2\hat{\varphi}_{1,j} &= k_0^2(1-a_1V_b)\hat{\psi}_j - \zeta k_0^2(1-b_1V_b)\hat{\varphi}_{1,j},\\
-a_l D_h^2\hat{\varphi}_{l-1,j} + b_l D_h^2\hat{\varphi}_{l,j} &= k_0^2(1-a_lV_b)\hat{\varphi}_{l-1,j} - k_0^2(1-b_1V_b)\hat{\varphi}_{l,j},\\
&\qquad l = 2,\ldots,p-1,\\
-\frac{c_U}{c_W}a_p D_h^2\hat{\varphi}_{p-1,j} + b_p D_h^2\hat{\psi}_j &= \frac{c_U}{c_W}k_0^2(1-a_pV_b)\hat{\varphi}_{p-1,j} - k_0^2(1-b_pV_b)\hat{\psi}_j.
\end{aligned} \tag{24}$$

We rewrite the transformed system (24) in matrix notation as

$$\mathbf{X}\Delta^+\Delta^-\hat{\boldsymbol{\psi}}_j = \mathbf{Y}\hat{\boldsymbol{\psi}}_j, \qquad j \geq J, \tag{25}$$

where we defined the vector $\hat{\boldsymbol{\psi}}_j := (\hat{\psi}, \hat{\varphi}_1, \ldots, \hat{\varphi}_{p-1})_j^\top \in \mathbb{C}^p$ and the complex $p \times p$–matrices

$$\mathbf{X} := \begin{pmatrix}
-a_1 & \zeta b_1 & & & \\
 & -a_2 & b_2 & & \\
 & & \ddots & \ddots & \\
 & & & -a_{p-1} & b_{p-1}\\
b_p & & & & -\frac{c_U}{c_W}a_p
\end{pmatrix}$$

and

$$\mathbf{Y} := h^2k_0^2 \begin{pmatrix} 1-a_1V_b & -\zeta(1-b_1V_b) & & & \\ & 1-a_2V_b & -(1-b_2V_b) & & \\ & & \ddots & \ddots & \\ & & & 1-a_{p-1}V_b & -(1-b_{p-1}V_b) \\ -(1-b_pV_b) & & & & \frac{c_U}{c_W}(1-a_pV_b) \end{pmatrix}.$$

Here, Δ^+, Δ^- denote the standard forward and backward difference operators

$$\Delta^+\hat{\boldsymbol{\psi}}_j = \hat{\boldsymbol{\psi}}_{j+1} - \hat{\boldsymbol{\psi}}_j, \qquad \Delta^-\hat{\boldsymbol{\psi}}_j = \hat{\boldsymbol{\psi}}_j - \hat{\boldsymbol{\psi}}_{j-1}.$$

By introducing $\hat{\boldsymbol{\xi}}_j := \Delta^-\hat{\boldsymbol{\psi}}_j$ we rewrite (25) as a system of 2p first order difference equations

$$\underbrace{\begin{pmatrix} \mathbf{0} & \mathbf{X} \\ \mathbf{I} & -\mathbf{I} \end{pmatrix}}_{\mathbf{A}} \Delta^+ \begin{pmatrix} \hat{\boldsymbol{\psi}}_j \\ \hat{\boldsymbol{\xi}}_j \end{pmatrix} = \underbrace{\begin{pmatrix} \mathbf{Y} & \mathbf{0} \\ \mathbf{0} & \mathbf{I} \end{pmatrix}}_{\mathbf{B}} \begin{pmatrix} \hat{\boldsymbol{\psi}}_j \\ \hat{\boldsymbol{\xi}}_j \end{pmatrix},$$

i.e.

$$\begin{pmatrix} \Delta^+\hat{\boldsymbol{\psi}}_j \\ \Delta^+\hat{\boldsymbol{\xi}}_j \end{pmatrix} = \mathbf{A}^{-1}\mathbf{B} \begin{pmatrix} \hat{\boldsymbol{\psi}}_j \\ \hat{\boldsymbol{\xi}}_j \end{pmatrix} \quad \text{or} \quad \begin{pmatrix} \hat{\boldsymbol{\psi}}_{j+1} \\ \hat{\boldsymbol{\xi}}_{j+1} \end{pmatrix} = (\mathbf{A}^{-1}\mathbf{B} + \mathbf{I}) \begin{pmatrix} \hat{\boldsymbol{\psi}}_j \\ \hat{\boldsymbol{\xi}}_j \end{pmatrix}, \quad j \geq J\,.$$

Let us briefly comment of the regularity of $\mathbf{A}$, i.e. of $\mathbf{X}$. One easily computes

$$\det \mathbf{X} = (-1)^p \frac{c_U}{c_W} \prod_{l=1}^{p} a_l - \zeta \prod_{l=1}^{p} b_l$$

which vanishes for exactly one value of ζ. Hence $\mathbf{A}^{-1} = \left(\begin{smallmatrix} \mathbf{X^{-1}} & \mathbf{I} \\ \mathbf{X^{-1}} & \mathbf{0} \end{smallmatrix}\right)$ exists for ζ chosen sufficiently large.

We split the Jordan form $\mathbf{J} = \mathrm{diag}(\mathbf{J_1}, \mathbf{J_2})$ of $\mathbf{A}^{-1}\mathbf{B}+\mathbf{I}$, $\mathbf{J}_1 \in \mathbb{C}^{p\times p}$ containing the Jordan blocks corresponding to solutions decaying for $j \to \infty$ and $\mathbf{J}_2 \in \mathbb{C}^{p\times p}$ those which increase. With the matrix of left eigenvectors $\mathbf{P}^{-1} = \left(\begin{smallmatrix} \mathbf{P}_1 & \mathbf{P}_2 \\ \mathbf{P}_3 & \mathbf{P}_4 \end{smallmatrix}\right)$ the equation

$$\begin{aligned} \mathbf{P}^{-1} \begin{pmatrix} \hat{\boldsymbol{\psi}}_{j+1} \\ \hat{\boldsymbol{\xi}}_{j+1} \end{pmatrix} &= \mathbf{P}^{-1}(\mathbf{A}^{-1}\mathbf{B} + \mathbf{I}) \begin{pmatrix} \hat{\boldsymbol{\psi}}_j \\ \hat{\boldsymbol{\xi}}_j \end{pmatrix} = \mathbf{P}^{-1}\mathbf{P} \begin{pmatrix} \mathbf{J}_1 & \mathbf{0} \\ \mathbf{0} & \mathbf{J}_2 \end{pmatrix} \begin{pmatrix} \mathbf{P}_1 & \mathbf{P}_2 \\ \mathbf{P}_3 & \mathbf{P}_4 \end{pmatrix} \begin{pmatrix} \hat{\boldsymbol{\psi}}_j \\ \hat{\boldsymbol{\xi}}_j \end{pmatrix} \\ &= \begin{pmatrix} \mathbf{J}_1 & \mathbf{0} \\ \mathbf{0} & \mathbf{J}_2 \end{pmatrix} \begin{pmatrix} \mathbf{P}_1\hat{\boldsymbol{\psi}}_j + \mathbf{P}_2\hat{\boldsymbol{\xi}}_j \\ \mathbf{P}_3\hat{\boldsymbol{\psi}}_j + \mathbf{P}_4\hat{\boldsymbol{\xi}}_j \end{pmatrix} \end{aligned}$$

holds and thus the *transformed DTBC* reads

$$\mathbf{P}_3\hat{\boldsymbol{\psi}}_J + \mathbf{P}_4\hat{\boldsymbol{\xi}}_J = 0.$$

For a regular matrix $\mathbf{P}_4$ the $\mathcal{Z}$–transformed DTBC can be written in Dirichlet-to-Neumann form

$$\Delta^-\hat{\boldsymbol{\psi}}_J = \widehat{\mathbf{D}}\hat{\boldsymbol{\psi}}_J\,,$$

where $\widehat{\mathbf{D}} = -(\mathbf{P}_4)^{-1}\mathbf{P}_3$. Finally, an inverse $\mathcal{Z}$–transformation yields the *DTBC*

$$\boldsymbol{\psi}_J^{n+1} - \boldsymbol{\psi}_{J-1}^{n+1} - \mathbf{D}^0\boldsymbol{\psi}_J^{n+1} = \sum_{l=1}^{n}\mathbf{D}^{n+1-l}\boldsymbol{\psi}_J^l\,. \tag{26}$$

with the convolution coefficients given by the Cauchy integral formula

$$\mathbf{D}^n = \mathcal{Z}^{-1}\{\widehat{\mathbf{D}}(z)\} = \frac{\tau^n}{2\pi}\int_0^{2\pi}\widehat{\mathbf{D}}(\tau e^{i\varphi})e^{in\varphi}\,d\varphi, \quad n\in\mathbb{Z}_0, \quad \tau>0.$$

Since this inverse $\mathcal{Z}$-transformation cannot be done explicitly, we use a numerical inversion technique based on FFT (cf. [14]); for details of this routine (especially the choice of the inversion radius τ) we refer the reader to [48].

So far we did not consider the (typical) *density jump* at the sea bottom at $z = z_b$. In the following we review a possible discretization of the water–bottom interface. For our grid z_j, $j\in\mathbb{N}_0$ with $Jh = z_b$ the discontinuity of ρ is located at the grid point z_J. In this case it is a standard practice [37] to use (16) with

$$\rho_j = \begin{cases}\rho_w, & j<J,\\ \frac{2\,\rho_b\rho_w}{\rho_b+\rho_w}, & j=J,\\ \rho_b, & j>J.\end{cases} \tag{27}$$

and apply the DTBC (26) in the sea bottom at the grid points z_{J+2}, z_{J+3} (instead of z_{J-1}, z_J). For a detailed discussion of various strategies of an adequate discrete treatment of the density shock at $z = z_b$ we refer to [3].

6.2 The DTBC for the split–step Padé algorithm

Now let us describe briefly the differences in the derivation of the DTBC for the split–step Padé algorithm. To do so, we consider the scheme (14) with the depth discretization from §5 (or simply (16)) in the exterior domain $j\geq J$ and drop for convenience the second index p:

$$\psi_j^{n+1} = \left(1 + \sum_{l=1}^{p}\frac{a_l L_h}{1+b_l L_h}\right)\psi_j^n, \qquad n\geq 0.$$

Next we introduce the intermediate functions $\varphi_1^{n+1}(z), \ldots, \varphi_{p-1}^{n+1}(z)$ that fulfill

$$\varphi_{l,j}^{n+1} = \frac{a_l L_h}{1 + b_l L_h} \psi_j^n, \qquad l = 1, \ldots, p-1,$$
$$\psi_j^{n+1} - \sum_{l=1}^{p-1} \varphi_{l,j}^{n+1} = \left(1 + \frac{a_p L_h}{1 + b_p L_h}\right) \psi_j^n.$$

We apply the $\mathcal{Z}$–transformation (23) which yields the following $\mathcal{Z}$–transformed system

$$\mathbf{X}\Delta^+\Delta^- \hat{\boldsymbol{\psi}}_j = \mathbf{Y}\hat{\boldsymbol{\psi}}_j, \qquad j \geq J,$$

where we defined the vector $\hat{\boldsymbol{\psi}}_j = (\hat{\psi}, \hat{\varphi}_1, \ldots, \hat{\varphi}_{p-1})_j^\top \in \mathbb{C}^p$ and the complex $p \times p$–matrices

$$\mathbf{X} := \begin{pmatrix} -\frac{a_1}{\zeta} & b_1 & & \\ \vdots & & \ddots & \\ -\frac{a_{p-1}}{\zeta} & & & b_{p-1} \\ b_p - \frac{a_p}{\zeta - 1} & -\frac{\zeta b_p}{\zeta - 1} & \cdots & -\frac{\zeta b_p}{\zeta - 1} \end{pmatrix}$$

and

$$\mathbf{Y} := h^2 k_0^2 \begin{pmatrix} -\frac{a_1 V_b}{\zeta} & b_1 V_b + 1 & & \\ \vdots & & \ddots & \\ -\frac{a_{p-1} V_b}{\zeta} & & & b_{p-1} V_b + 1 \\ 1 + (b_p - \frac{a_p}{\zeta - 1}) V_b & \frac{-\zeta}{\zeta - 1}(1 + b_p V_b) & \cdots & \frac{-\zeta}{\zeta - 1}(1 + b_p V_b) \end{pmatrix}.$$

The invertibility of $\mathbf{X}$ follows from

$$\det \mathbf{X} = (-1)^{p+1} \prod_{l=1}^{p} b_l + \frac{1}{\zeta - 1} \sum_{l=1}^{p} (-1)^{q_l(p)} a_l \prod_{\substack{m=1 \\ m \neq l}}^{p} b_m$$

(with some signature function $q_l(p)$) for ζ chosen sufficiently large. The remaining part of the construction is completely analogous to the preceding §6.1.

7 Numerical Examples

In our examples we shall consider higher–order approximants to the one–way Helmholtz equation illustrating the numerical results when using the discrete TBCs of §6. We emphasize that, due to its construction, our discrete TBC yields exactly (up to round–off errors and evanescent errors in the numerical

inverse $\mathcal{Z}$–transformation) the numerical solution on the unbounded domain restricted to the finite computational interval.

7.1 Example 1

In the first example we choose the benchmark data arising in optics from [20], [42] to duplicate and compare the numerical results with our method. The computational domain is $\Omega = (-50, 50) \times (0, 400)\,\mu\text{m}^2$. As a starting field we use a Gaussian input beam of the form

$$\psi^I(z) = \psi(z, 0) = \exp\{ik_0 z \sin\phi - (z/10)^2\}, \quad |z| < 50\,\mu\text{m},$$

where ϕ denotes the angle between propagation direction and the r–axis. We consider two dimensional plain wave propagation in a homogeneous medium, i.e. the potential term is zero: $V \equiv 0$ and $k_0 = 2\pi/\lambda$ with the free space wavelength $\lambda = 1.55\,\mu\text{m}$. We compute the field from $r = 0$ to $r = 400\,\mu\text{m}$ using the propagation step size $k = \Delta r = 0.4\,\mu\text{m}$ (i.e. 1000 steps). The transverse grid spacing is taken to be $h = \Delta z = 0.2\,\mu\text{m}$. In this example we need two DTBCs at the left and right endpoint of the computational z-interval. The DTBC at the left endpoint $z_L = -50\,\mu\text{m}$ is derived analogously.

In our first numerical example we add two Gaussian beams with the propagation angles $\phi = \pi/4$ and $\phi = -\pi/4$ and normalize the initial data $\psi_j^0 = \psi^I(z_L + jh)$, $j = 0, 1 \ldots, J$, (with $Jh = z_R = 50\,\mu\text{m}$), such that $\|\psi^0\|_2 = 1$. Here the discrete ℓ^2–norm on the computational interval is defined by

$$\|\psi^n\|_2^2 = h \sum_{j=1}^{J-1} |\psi_j^n|^2, \qquad n \geq 0. \tag{28}$$

This propagation experiment of two beams with a relative angle of $\pi/2$ needs essentially the wide–angle property of higher–order approximants since otherwise considerable *phase errors* are induced (cf. the detailed analysis in [42]).

7.1.1 The Split–Step High–Order PE Method

We consider the split–step algorithm (11) with the discrete depth operator (16) for solving the high–order parabolic equations of §2. To treat the wide–angle propagation we use a (4,4)–Padé approximation (the same was done in [42]). Fig. 2 shows the solution with the high–order PE method and expresses the fact that this very wide–angle propagation problem can be solved with the proposed method.

Next we want to draw the readers's attention to the high *accuracy* of the discrete TBCs. In Fig. 3 we display the discrete ℓ^2–norm of the solution as a

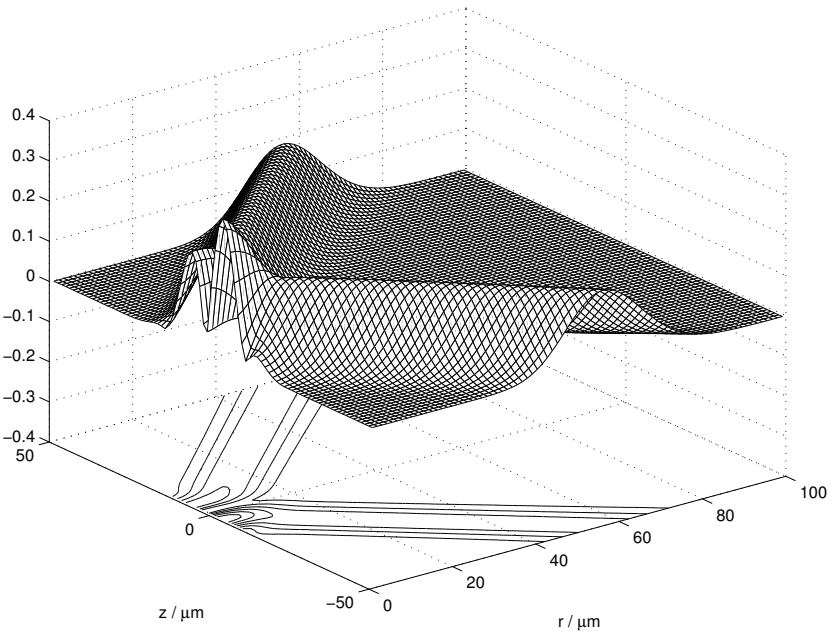

Fig. 2. Propagation of two Gaussian beams at a relative angle of $\pi/2$.

function of r and varying step sizes h. We point out that in all our simulations unphysical numerical plateaus (like in [42]) do not appear (independent from the chosen transverse step size h). Hence our fully discrete approach for deriving TBCs seems to be more appropriate (at about the same computational costs) for pure wave propagation problems than the semi–discrete approach of [42].

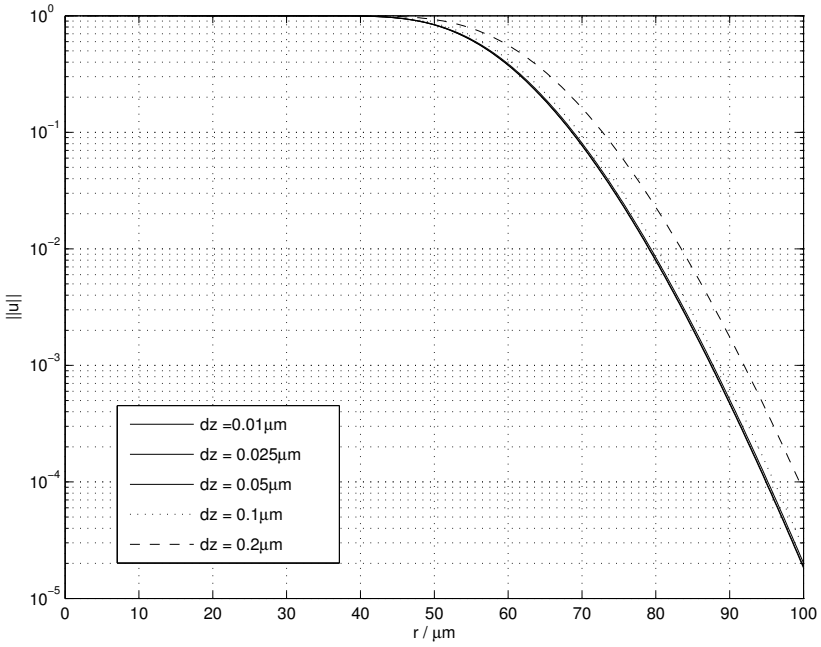

Fig. 3. The discrete ℓ^2–norm (28) of the solution for the propagation range $0 \leq r \leq 400\,\mu$m and varying transverse step sizes Δz.

In Fig. 4 we consider an (8,8)–Padé approximation, enlarged the propagation range up to $400\,\mu$m and used the coarse transverse step size $h = 0.2\,\mu$m in order to investigate the long range behaviour and thus the stability of our algorithm. Again, one observes no reflected fields (i.e. plateaus) in the curve. After the wave packet has left the computational domain only some numerical 'noise' of magnitude 10^{-12} remains.

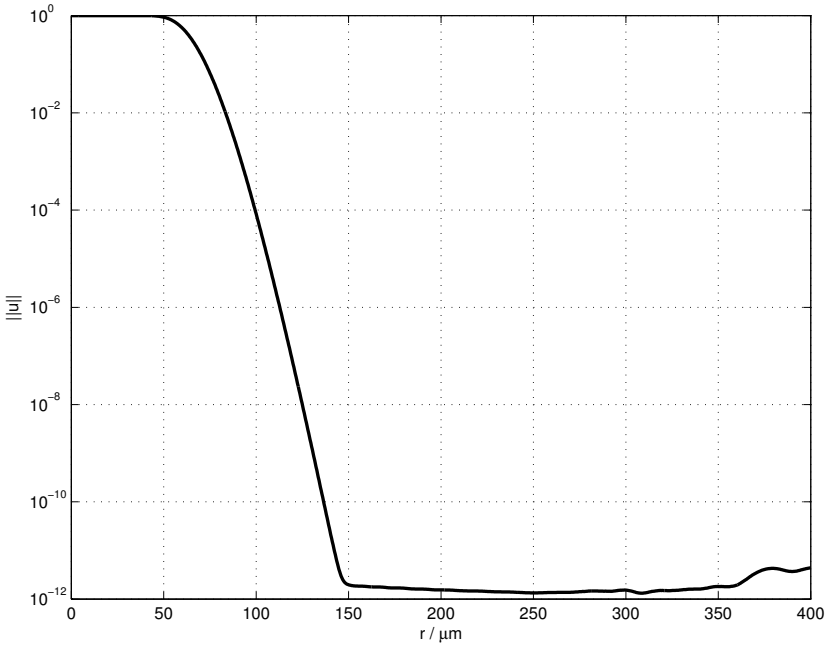

Fig. 4. The discrete ℓ^2–norm of the solution of (8,8)–propagator for $0 \leq r \leq 400\,\mu$m and $\Delta z = 0.2\,\mu$m.

To obtain a more quantitative result about the error induced by the DTBCs we compute a reference solution on a three times larger z–domain and plot the discrete ℓ^2–norm of the error in Fig. 5. The order of magnitude of the error is 10^{-14} which is around the order of the roundoff error and is orders of magnitudes smaller than the order of the discretization error.

7.1.2 The Split–Step Padé Method

Now we turn to the second presented numerical scheme, the split–step Padé method of §4 with the depth operator from §5, and repeat the calculations. We use the same discretization parameters as before and choose $p = 4$ in (14). Fig. 6 shows the solution and one can recognize that the phase error is smaller than using the method of §7.1.1 since the peak of the wave should leave the computational domain at $z_R = 50\,\mu$m. We turn to the accuracy of the discrete TBC for the Split–Step Padé method and plot in Fig. 7 the discrete ℓ^2–norm of the solution for the same step sizes h as in Fig. 3. Again no numerical plateaus emerged and the curves for the different transverse step sizes Δz are

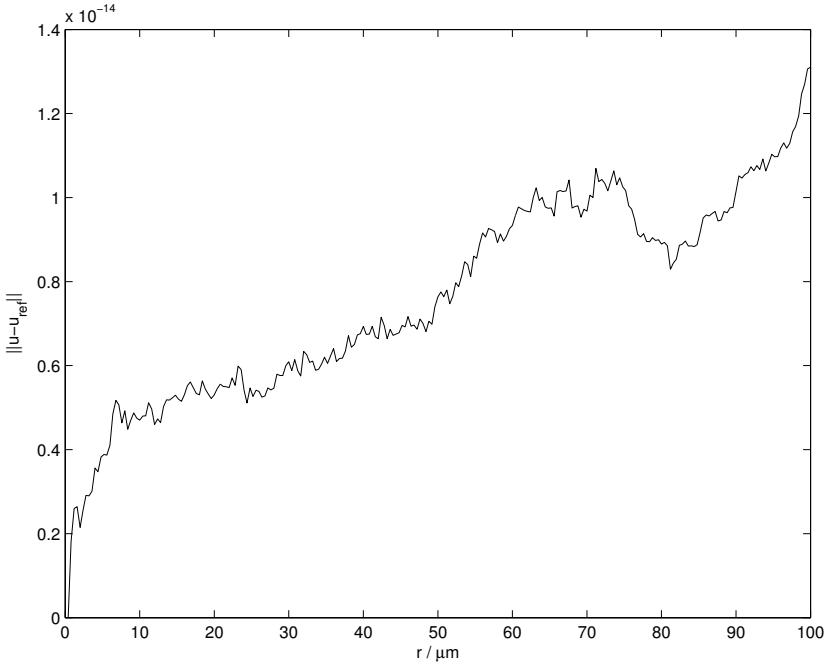

Fig. 5. The discrete ℓ^2–norm of the error (observe the scaling!)

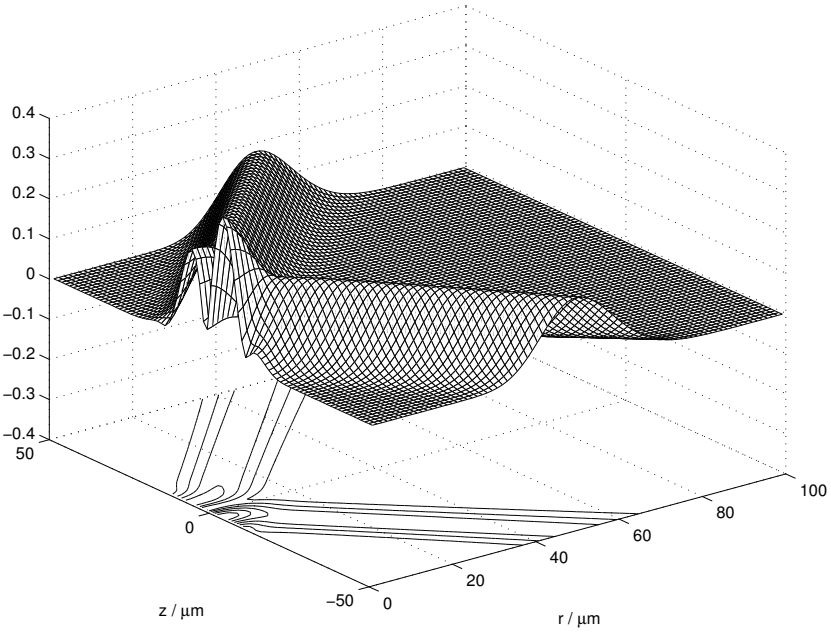

Fig. 6. Split–Step Padé method: Propagation of two Gaussian beams at a relative angle of $\pi/2$.

indistinguishable. In Fig. 8 we computed the solution up to $400\,\mu$m with the coarse transverse step size $h = 0.2\,\mu$m and the curve reveals no numerical plateaus. The discrete ℓ^2–norm of the error due to the DTBC in Fig. 9 is even smaller than the error in Fig. 5.

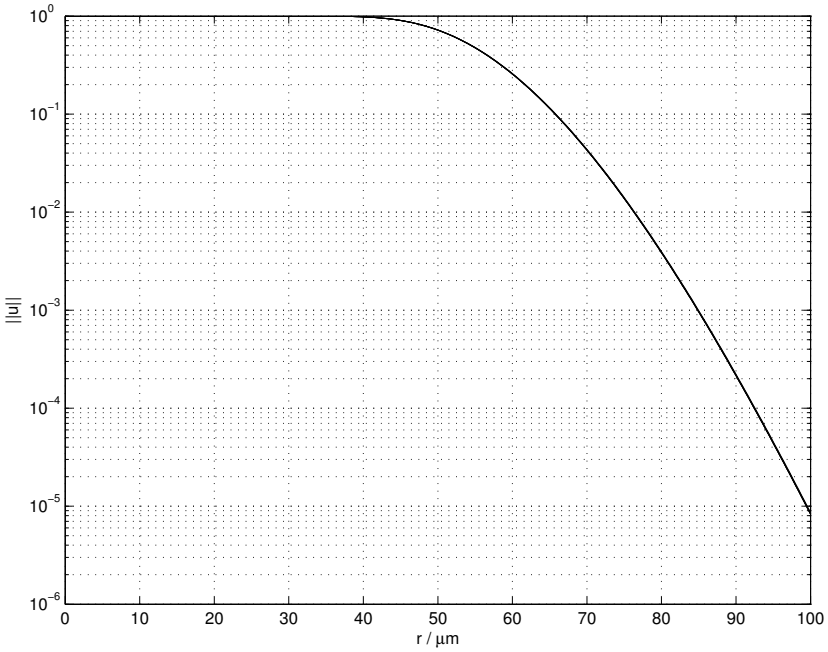

Fig. 7. Split–Step Padé method: The discrete ℓ^2–norm of the solution for $0 \leq r \leq 400\,\mu$m and varying step sizes Δz.

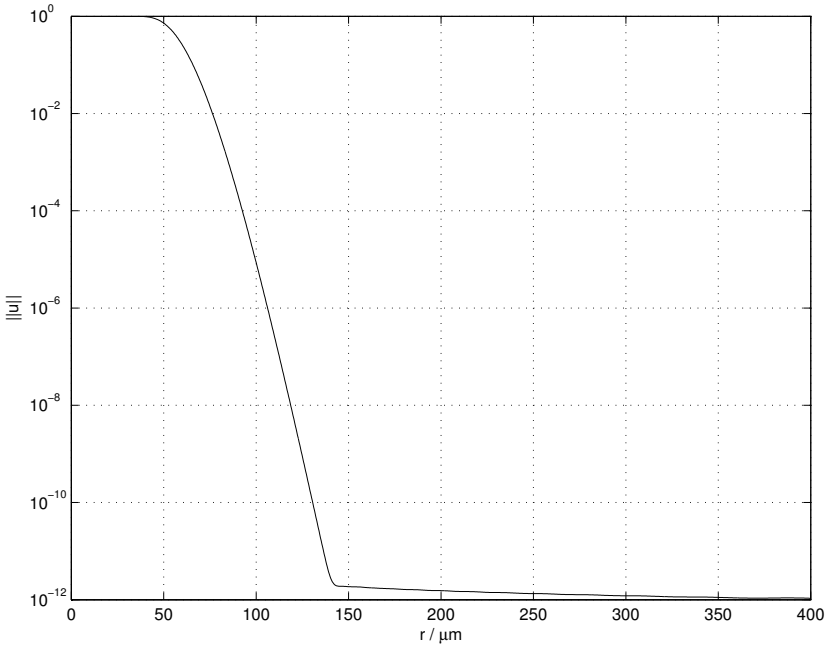

Fig. 8. Split–Step Padé method: The discrete ℓ^2–norm of the solution for $0 \leq r \leq 400\,\mu$m and $\Delta z = 0.2\,\mu$m.

Finally, we compare directly the results using the split–step algorithm (11) and split–step Padé method of Collins with the depth operator from §5 and the standard transverse operator (16). In Fig. 10 we plot again the discrete ℓ^2–norm of the solution and it is apparent that one has to use a small transverse

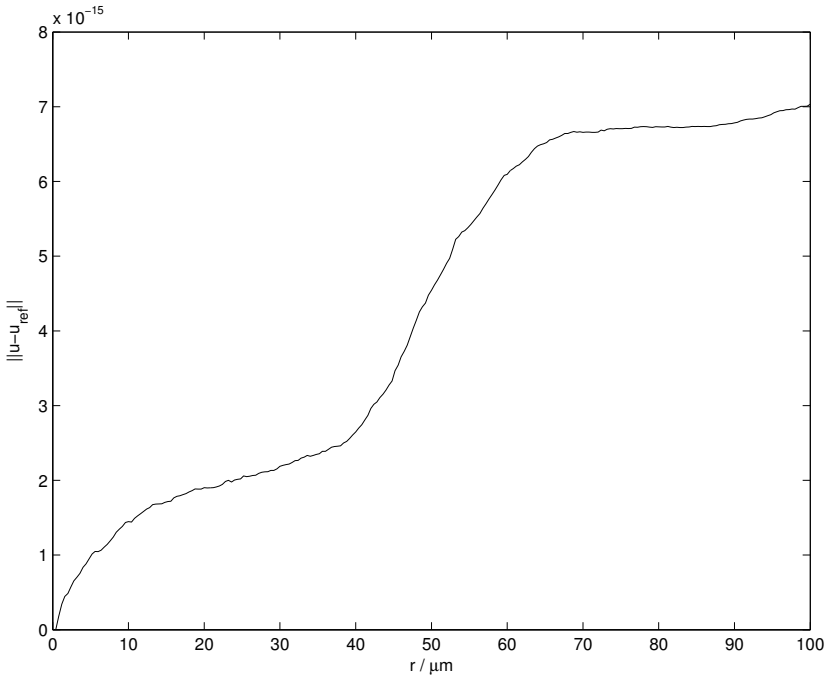

Fig. 9. Split–Step Padé method: The discrete ℓ^2–norm of the error.

step size in the first method (11) to obtain results comparable to the split–step Padé method. Thus the split–step Padé solution method (14) with the depth operator of §5 gives the best results for this example.

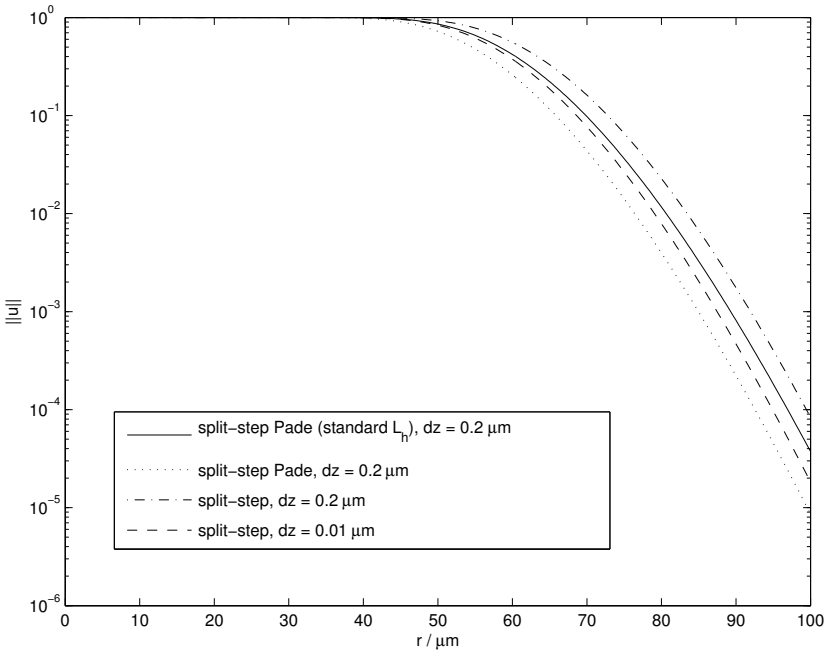

Fig. 10. Comparison of the discrete ℓ^2–norm of the solution for both approaches

7.2 Example 2

This example from underwater acoustics is closely related to the example A of [10]. In this example the ocean region ($0 < z < 200\,\mathrm{m}$) with the uniform density $\rho_w = 1.0\,\mathrm{gcm}^{-3}$ is modeled by the one–way Helmholtz equation (3). It contains no attenuation in the water $\alpha_w = 0\,\mathrm{dB}\,/\lambda$, and the attenuation in the bottom is $\alpha_b = 0.5\,\mathrm{dB}\,/\lambda$, $\lambda = c(z)/f$. There is a large density jump ($\rho_b = 1.5\,\mathrm{gcm}^{-3}$) at the water–bottom interface at $z_b = 200\,\mathrm{m}$.

The source of $f = 25\,\mathrm{Hz}$ is located at a water depth $z_s = 100\,\mathrm{m}$ and the receiver depth is at $z_r = 30\,\mathrm{m}$. For the sound speed in the water we assume $c(z) \equiv c_0 = 1500\,\mathrm{ms}^{-1}$ and the sound speed in the bottom is $c_b = 1700\,\mathrm{ms}^{-1}$. For our calculations with the split–step Padé method of Collins up to a maximum range of 10 km we used a uniform computational grid with depth step $h = \Delta z = 2\,\mathrm{m}$ and different range steps $k = \Delta r$. Here we employ the Gaussian beam from [32] as a starting field $\psi^I = \psi(z, 0)$.

Below we present the so–called *transmission loss* $TL(r) := -10\log_{10}|p(z_r, r)|^2$, where the acoustic pressure p is calculated from (2). We computed a densely sampled *comparison solution* using the range step $k = 50\,\mathrm{m}$ and sparsely sampled solutions for $p = 4$, $k = 200\,\mathrm{m}$ and for $p = 8$ $k = 400\,\mathrm{m}$. In Fig. 11 and Fig. 12 one observes that both of the sparsely sampled split–step Padé solutions are in good agreement with the dense solutions and thus in many applications are large a range step can be used with this method.

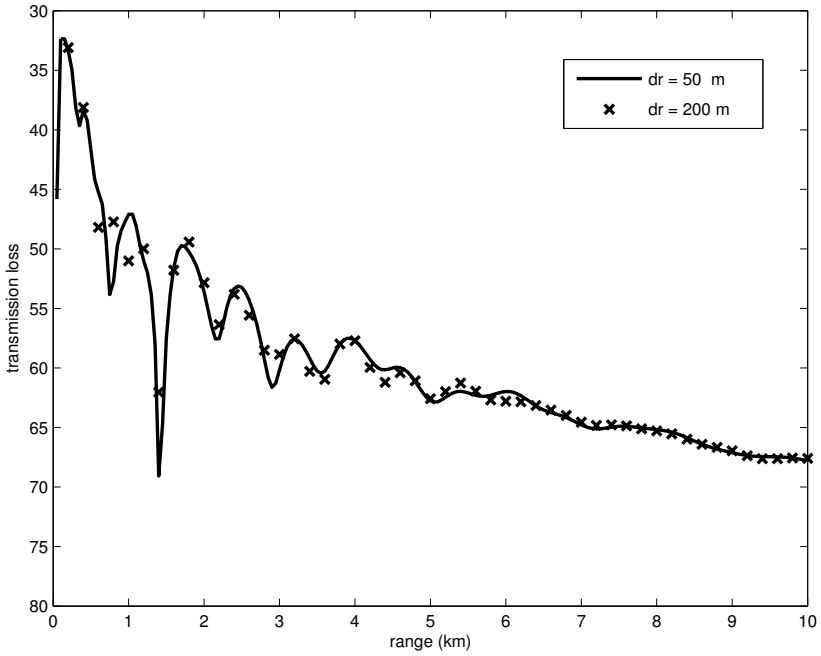

Fig. 11. Transmission loss at $z_r = 30\,\mathrm{m}$: densely sampled comparison solution and sparsely sampled solution for $p = 4$ and $k = 200\,\mathrm{m}$.

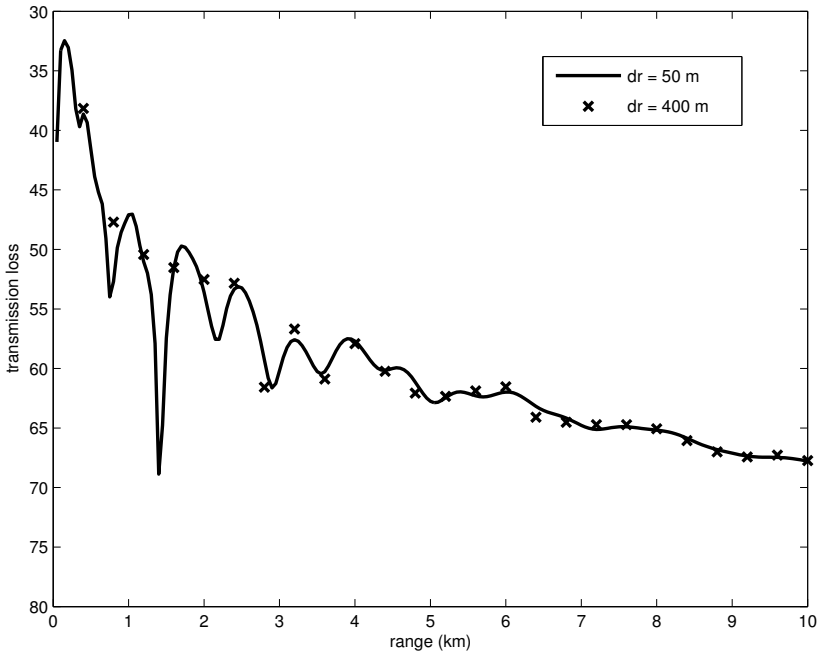

Fig. 12. Transmission loss at $z_r = 30\,\mathrm{m}$: densely sampled comparison solution and sparsely sampled solution for $p = 8$ and $k = 400\,\mathrm{m}$.

Finally we compute a solution for $p = 8$ and $k = 400\,\mathrm{m}$ on a three times larger z–domain confined with the DTBC and determined the discrete ℓ^2–norm of the error in Fig. 13. The order of magnitude of the error due to the DTBC is 10^{-12} (for $p = 4$ and $k = 400\,\mathrm{m}$ it is 10^{-15}) which is negligible compared to the discretization error. We remark that the residuals when computing the Padé coefficients in (20) with the MATLAB routine `fsolve` are 10^{-6} for $p = 8$, $k = 400\,\mathrm{m}$ and 10^{-12} for $p = 4$, $k = 200\,\mathrm{m}$.

Conclusions

We have derived exact discrete transparent boundary conditions for different rational approximations to the one–way Helmholtz equation. This approach generalizes substantially our work [3] for the case of a (1,1)–Padé approximant. In the numerical example without potential term our DTBC for the split–step algorithm for the high–order PE outperformed the previously derived semi–discrete TBC [42] and showed no numerical plateaus. It turned out that the split–step Padé solution method of Collins [10] with the depth operator of §5 provided the most accurate results for this example. However, it is unclear how to generalize this depth operator to the case of a non–zero potential term. We believe that this general approach will be valuable for many applications arising in two–dimensional scalar wave propagation problems, e.g. it can implemented into the *Range–dependent Acoustic Model* (RAM) code [11].

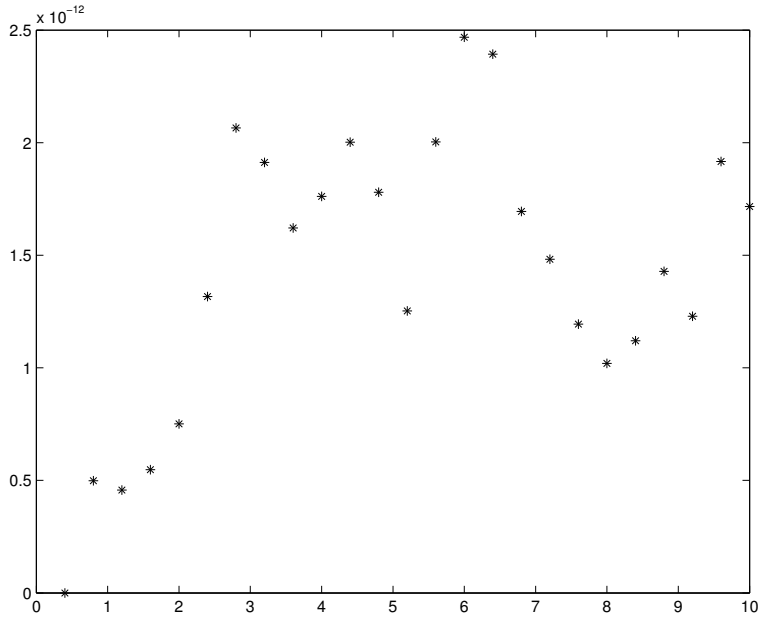

Fig. 13. The discrete ℓ^2–norm of the error for the case $p = 8$ and $k = 400\,\mathrm{m}$.

Future work will be concerned with the stability proofs of the two presented methods and the implementation and analysis of the *sum–of–exponentials approximation* [15] to the discrete convolution–type transparent boundary condition in order to further improve the efficiency of our approach.

References

[1] S. Amini and S.M. Kirkup, *Solution of Helmholtz equation in the exterior domain be elementary boundary integral methods*, J. Comp. Phys. **118** (1995), 208–221.

[2] A. Arnold, *Numerically Absorbing Boundary Conditions for Quantum Evolution Equations*, VLSI Design **6** (1998), 313–319.

[3] A. Arnold and M. Ehrhardt, *Discrete transparent boundary conditions for wide angle parabolic equations in underwater acoustics*, J. Comp. Phys. **145** (1998), 611–638.

[4] A. Bamberger, B. Engquist, L. Halpern and P. Joly, *Higher order paraxial wave equation approximations in heterogeneous media*, SIAM J. Appl. Math. **48** (1988), 129–154.

[5] V.A. Baskakov and A.V. Popov, *Implementation of transparent boundaries for numerical solution of the Schrödinger equation*, Wave Motion **14** (1991), 123–128.

[6] J.-P. Bérenger, *A perfectly matched layer for the absorption of electromagnetic waves*, J. Comp. Phys. **114** (1994), 185–200.

[7] H.K. Brock, *The AESD parabolic equation model*, Report TN–12, Naval Ocean Research and Development Activity, Stennis Space Center, MS, 1978.

[8] G.H. Brooke and D.J. Thomson, *Non–local boundary conditions for high–order parabolic equation algorithms*, Wave Motion **31** (2000), 117–129.

[9] J.F. Claerbout, *Coarse grid calculation of waves in inhomogeneous media with application to delineation of complicated seismic structure*, Geophysics **35** (1970), 407–418.

[10] M.D. Collins, *A split–step Padé solution for the parabolic equation method*, J. Acoust. Soc. Am. **93** (1993), 1736–1742.

[11] M.D. Collins, *User's Guide for RAM Versions 1.0 and 1.0p*, Naval Research Laboratory, Washington, D.C, 1997.

[12] T.W. Dawson, G.H. Brook and D.J. Thomson, *Exact boundary conditions for acoustic PE modeling over an N^2–linear half–space*, submitted to: J. Acoust. Soc. Am.

[13] G. Doetsch, *Anleitung zum praktischen Gebrauch der Laplace–Transformation und der $\mathcal{Z}$–Transformation*, R. Oldenburg Verlag, 3. Auflage 1967.

[14] M. Ehrhardt and A. Arnold, *Discrete Transparent Boundary Conditions for the Schrödinger Equation*, Riv. Mat. Univ. Parma **6** (2001), 57–108.

[15] M. Ehrhardt and A. Arnold, *Discrete Transparent Boundary Conditions for Wide Angle Parabolic Equations: Fast Calculation and Approximation*, in *Proceedings of the Seventh European Conference on Underwater Acoustics*, July 3–8, 2004, Delft, The Netherlands, pp. 9–14.

[16] M. Ehrhardt and R.E. Mickens, *Solutions to the Discrete Airy Equation: Application to Parabolic Equation Calculations*, J. Comput. Appl. Math. **172** 2004, 183–206.

[17] M. Ehrhardt, *Discrete Transparent Boundary Conditions for Wide Angle Parabolic equations for non–vanishing starting fields*, Preprint No. 221 of the DFG Research Center MATHEON Berlin, March 2005.

[18] M.D. Feit and J.A. Fleck, *Light propagation in graded–index optical fibers*, Appl. Opt. **17** (1978), 3990–3997.

[19] S.M. Flatté and F.D. Tappert, *Calculations of the effect of internal waves on oceanic sound transmission*, J. Acoust. Soc. Am. **58** (1975), 1151–1159.

[20] T. Friese, F. Schmidt and D. Yevick, *Transparent boundary conditions for a wide–angle approximation of the one–way Helmholtz equation*, J. Comp. Phys. **165** (2000), 645–659.

[21] K. Gerdes and L. Demkovicz, *Solutions of 3D–Laplace and Helmholtz equations in exterior domains using hp infinite elements*, Comp. Methods Appl. Mech. Eng. **137** (1996), 239–273.

[22] W.B. Gragg and G.D. Johnson, *The Laurent–Padé table*, in: Information Processing **74**, North–Holland, Amsterdam, 1974, pp. 632–637.

[23] R.R. Greene, *The rational approximation to the acoustic wave equation with bottom interaction*, J. Acoust. Soc. Am. **76** (1984), 1764–1773.

[24] O.A. Godin, *Reciprocity and energy conservation within the parabolic approximation*, Wave Motion **29** (1999), 175–194.

[25] L. Halpern and L.N. Trefethen, *Wide–Angle one–way wave equations*, J. Acoust. Soc. Am. **84** (1988), 1397–1404.

[26] R.H. Hardin and F.D. Tappert, *Applications of the split–step Fourier method to the numerical solution of nonlinear and variable coefficient wave equations*, SIAM Rev. **15** (1973), 423.

[27] J.R. Hellums and W.R. Frensley, *Non–Markovian open–system boundary conditions for the time–dependent Schrödinger equation*, Phys. Rev. B **49** (1994), 2904–2906.

[28] F.B. Jensen, W.A. Kuperman, M.B. Porter and H. Schmidt, *Computational Ocean Acoustics*, AIP Press, New York, 1994.

[29] N.A. Kampanis, *A finite element method for the parabolic equation in aeroacoustics coupled with a nonlocal boundary condition for an inhomogeneous atmosphere*, J. Comput. Acoust., accepted for publication.

[30] J.B. Keller and D. Givoli, *Exact non–reflecting boundary conditions*, J. Comp. Phys. **82** (1989), 172–192.

[31] G.H. Knightly, D. Lee and D.F. St. Mary, *A Higher–Order Parabolic Wave Equation*, J. Acoust. Soc. Am. **82** (1987), 580–587.

[32] D. Lee and S.T. McDaniel, *Ocean acoustic propagation by finite difference methods*, Comput. Math. Appl. **14** (1987), 305–423.

[33] M.A. Leontovich and V.A. Fock, *Solution of propagation of electromagnetic waves along the earth's surface by the method of parabolic equations*, J. Phys. USSR **10** (1946), 13–23.

[34] M.F. Levy, *Parabolic equation models for electromagnetic wave propagation*, (IEE Electromagnetic Waves Series 45, 2000).

[35] S.W. Marcus, *A generalized impedance method for application of parabolic approximation to underwater acoustics*, J. Acoust. Soc. Am. **90** (1991), 391–398.

[36] B. Mayfield, *Non–local boundary conditions for the Schrödinger equation*, Ph.D. thesis, University of Rhode Island, Providence, RI, 1989.

[37] S.T. McDaniel and D. Lee, *A finite–difference treatment of interface conditions for the parabolic wave equation: The horizontal interface*, J. Acoust. Soc. Am. **71** (1982), 855–858.

[38] D. Mikhin, *Exact discrete non–local boundary conditions for higher–order Padé parabolic equations*, J. Acoust. Soc. Am. **116** (2004), 2864–2875.

[39] J.S. Papadakis, *Impedance formulation of the bottom boundary condition for the parabolic equation model in underwater acoustics*, NORDA Parabolic Equation Workshop, NORDA Tech. Note 143, 1982.

[40] J.S. Papadakis, *Impedance Bottom Boundary Conditions for the Parabolic–Type Approximations in Underwater Acoustics*, in *Advances in Computer Methods for Partial Differential Equations VII*, eds. R. Vichnevetsky, D. Knight, and G. Richter, IMACS, New Brunswick, NJ, 1992, pp. 585–590.

[41] J.S. Papadakis, *Exact nonreflecting Boundary Conditions for parabolic–type approximations in underwater acoustics* J. Comput. Acous. **2** (1994), 83–98.

[42] F. Schmidt, T. Friese and D. Yevick, *Transparent Boundary Conditions for Split–Step Padé Approximations of the One–Way Helmholtz Equation*, J. Comp. Phys. **170** (2001), 696–719.

[43] F. Schmidt and P. Deuflhard, *Discrete transparent boundary conditions for the numerical solution of Fresnel's equation*, Comput. Math. Appl. **29** (1995), 53–76.

[44] F.D. Tappert, *The parabolic approximation method*, in *Wave Propagation and Underwater Acoustics*, Lecture Notes in Physics 70, eds. J.B. Keller and J.S. Papadakis, Springer, New York, 1977, pp. 224–287.

[45] L.N. Trefethen and L. Halpern, *Well–posedness of one–way wave equations and absorbing boundary conditions*, J. Acoust. Soc. Am. **47** (1986), 421–435.

[46] C. Vassalo, *Optical Waveguide Concepts*, Elsevier, 1991.

[47] D. Yevick and D.J. Thomson, *Complex Padé approximants for wide–angle acoustic propagators*, J. Acoust. Soc. Am. **108** (2000), 2784–2790.

[48] A. Zisowsky, *Discrete Transparent Boundary Conditions for Systems of Evolution Equations*, Ph.D. Thesis, Technische Universität Berlin, 2003.